SPACE SHUTTLE TECHNOLOGY

AERODYNAMICS

Arthur Henderson, Jr.
Langley Res. Center, NASA

Presented at the ELDO/NASA Space Transportation Systems Briefing
Bonn, Germany
July 7-8, 1970

Introduction

Certain elements within NASA have studied the aerothermodynamic aspects of space vehicle configuration design for many years. The advent of the Space Shuttle has furnished a focus to these studies that did not exist previously; and for the past year or more we have concentrated a large effort on exploring the aerothermodynamic characteristics of various Space Shuttle configuration concepts. During the course of these studies we have identified certain areas of concern which deserve particular attention. Some of these areas of concern are the focal point of the following presentation.

Figures 1 and 2 illustrate some of the orbiter and one of the booster concepts whose aerothermodynamic characteristics have been studied by NASA.

In addition to individual orbiter and booster studies, aerodynamic and heating characteristics of launch configurations have been explored.

Some of the areas of study upon which particular attention has been focused in the aerothermodynamic investigations are as outlined here.

One fact with which we are continually confronted is the unsatisfactory state of present day prediction techniques when applied to total configurational concepts. Newtonian or Newtonian-like methods continue to be used in the hypersonic flow regimes. The more elegant flow field calculation methods are being developed for simple geometric shapes; a more practical focus to this work would be of value to the configuration designer. The situation is less satisfactory in the transonic and subsonic flow regimes.

Most of our attention has been focused on the high heating rate portion of the vehicle--the lower surface. However, fluid dynamic studies on simple shapes have shown that, because of impingement of high energy vortical flow, there may be cause for concern--the so-called "shielded" upper surface may require more thermal protection than is currently estimated.

Experimental studies on the lee side of simple shapes have shown heating rates to be quite a bit higher than predicted on the basis of either separated flow or attached laminar flow. Since over half the surface area of shuttle vehicles is on the lee side, even small increases in thermal protection system unit weights can affect the total weight significantly. This potential area of concern requires further study; angle of attack and geometry dependence effects on heating rate need to be established, for instance.

That interference effects during launch can cause relatively large increases in local heating rates is illustrated. Note that the HL-10 is rear mounted, and that its nose is about mid-length of the booster, which is a region of low heating rate in the interference-free condition.

When, for the particular launch trajectory under consideration, the heating rates are converted to equilibrium wall temperatures, it is seen that the interference heating will cause no change in thermal protection system from that required for booster entry. However, as noted on the previous figure, the interference effects are superimposed on a region of low interference-free heating and the state of the boundary layer on the booster is laminar.

Many shuttle concepts will have the strong interference effects superimposed on regions of already high heating rate; and there is a possibility transitional or turbulent flow will exist in the important interference regions.

Launch configuration interference flow effects require much more study, not only from the heating standpoint, but also for drag loss, control and gimbal requirements, etc.

Some types of flow field interactions which can occur during a booster-orbiter separation maneuver are illustrated; flows vary from typical multiple shock boundary layer interactions to what appears to be a disgorged shock system similar to that for an unstarted supersonic inlet. Under normal staging conditions--high altitude, Mach number on the order of 10, and hence low dynamic pressure--the aerodynamics of the maneuver is not expected to play a major role. However, the aerodynamic interactions on the vehicles during an abort separation maneuver at low altitudes and high dynamic pressures may be a very hazardous operation.

The dependence of safe separation on the unknown dynamic damping derivatives is illustrated. The need for damping derivatives (or their equivalent effect) to be large is shown by comparing the minimum safe separation abscissa value with the estimated interference-free value for the same flight conditions. The feasibility of establishing the actual range of dynamic damping derivatives for both vehicles, where each vehicle is in the interference flow field of the other, has yet to be satisfactorily demonstrated.

The inputs to the solution of the equations of motion for the two-body system are all known, or are easily measured or calculated for a specific vehicle system, except the dynamic damping derivatives (underlined on the figure). Until the dynamic derivatives can be measured or estimated with reasonable accuracy, we can have little confidence in our ability to design for safe abort separation without resorting to brute force techniques, with their resultant penalties.

Jet impingement may add further complications to the booster-orbiter separation problem. This, superimposed on the already complex and time-varying interference flow fields, indicates that a high degree of ingenuity will be required if the vehicle separation problem is to be understood and resolved with adequate confidence.

The heating studies have generally been performed using the phase change coating technique (NASA TR R-230, February 1966). Time sequenced pictures of heating studies on a truncated model of the straight-wing orbiter are shown (model was truncated to obtain large scale in the region of interest--bow shock interactions with wing shock--and thus improve accuracy of data, while also avoiding tunnel blockage effects). Heat transfer coefficients at each point are found by measuring the time required for the melt line of the thin coating to reach that point.

Two strong interference flow regions are seen at both 20^{o} and 40^{o} angles of attack: one outboard on the wing due to bow shock-wing shock interaction, and one near the wing body juncture due to shock-boundary layer, and the viscous interactions caused by the differing wing and body boundary layer flow fields. Most of these interactions are absent at 60^{o} angle of attack: the wing shock is now detached so far from the wing that the bow shock-wing shock interaction has little effect on the wing.

Typical maximum equilibrium skin temperature distributions are shown for laminar boundary layer flow. Results were obtained from studies such as those on the previous figure in conjunction with a particular contractor-furnished entry trajectory.

The temperature distribution patterns on the body of the straight-wing orbiter suggest the presence of boundary layer transition. Evidence of the existence of transition is better seen on the following figure.

The variation of lower surface centerline heating rate on the straight-wing orbiter at $\alpha = 40^{\circ}$ is plotted against nondimensional distance from the nose of the truncated model for various free stream Reynolds numbers based on complete model length. As Reynolds number increases, boundary layer transition moves closer to the nose. Similar studies were performed at $\alpha = 20^{\circ}$.

Tabulated results indicate the existence of boundary layer transition Reynolds numbers, based on local conditions, lower than expected (s is surface distance from the Newtonian stagnation point to the beginning of transition). For example, at $\alpha = 40^{o}$, transition Reynolds numbers are all less than 200,000; these numbers are reminiscent of blunt body transition Reynolds numbers such as has been detected on Apollo.

Most boundary layer transition correlations that are presently being applied to Space Shuttle are based on simple configurations (flat plates, wedges, cones) at zero or low angles of attack. These existing correlations give conflicting predictions for conditions under which the Space Shuttle will operate. Transition will probably be dominated by cross-flow, pressure gradient, or geometry effects, which may cause the low transition Reynolds numbers observed. There is a need then, to assess the applicability of these existing correlations, and to attempt to determine more valid transition criteria for shuttle configurations.

Disturbances such as velocity, entropy, and density fluctuations often cause disparity between wind-tunnel and flight transition Reynolds number measurements, at least on the simple shapes

studied to date. However, the predominance of cross-flow, velocity gradient, and geometry effects may diminish the effects of tunnel-generated disturbances so that transition criteria based on wind-tunnel data may be more in accord with flight for shuttle applications. Concentrated research in this area is required.

Except for its relatively sharp nose, the planform of the General Dynamics/Convair orbiter is similar to that of the straight-wing orbiter. Yet the time sequenced phase change heating patterns show a marked difference in the manner in which transitional and turbulent flows develop on the two configurations. The effect of geometry on transition is pronounced.

The operational angle of attack range of the Space Shuttle may encompass angles from that for $(L/D)_{max}$ to $C_{L\ max}$ or greater. This figure illustrates the variation of cross flow characteristics for a portion of this range. Note that the presence of the wing interrupts the established forebody pattern, thus tending to make generalized studies on simple shapes of dubious value. An affirmative answer to the question "Can wind-tunnel studies be used with confidence for design of the Space Shuttle thermal protection system?" would be most welcome--we need an answer quickly.

Some previous figures have indicated both the presence and the effect upon heating distributions of interference flow fields. These electron beam flow visualization studies illustrate the variation of bow, wing, and tail shock shapes from 20° to 50° angles of attack. Although not seen in the figure, the interaction of bow and wing shock sends reflection waves back into the flow--it is possible that at certain angles of attack these disturbances can impinge on downstream control surfaces and affect the aerodynamic characteristics of the vehicle.

The complex nature of the flow field about the straight-wing orbiter is illustrated by these electron beam flow visualization studies. In each case the model is at 40° angle of attack; the vantage point from which the flow field is viewed varies.

An area of concern is that all interference flow studies to date have been performed in ideal gas facilities. The electron beam flow visualization was obtained in a helium tunnel with ratio of specific heats of 5/3; the heating studies were in ideal gas air tunnels with ratio of specific heats of 7/5. During entry, however, the maximum heat pulse will occur under the influence of real gas effects; effective ratio of specific heats will be in the 1.1 to 1.2 range. How do we interpret wind-tunnel results now? An answer to this question is overdue.

Concluding Remarks

The following areas of concern have been identified:

- Present day prediction techniques are not adequate for complete configuration design. The elegant methods which are being developed are applicable to simple geometries; they need to be attuned to the needs of total vehicle design.

- Lee side heating -- needs more definitive study for Space Shuttle candidates in operational modes.

- Launch interference heating -- Examine effect of relative fore and aft orbiter-booster locations. How will turbulent flow affect interference heating levels?

- Abort separation -- Dynamic damping derivatives are not known but have major effect on the separation maneuver; reliable measurement techniques must be devised.

- Boundary layer transition -- appears quite low. Are wind-tunnel results reasonably applicable to free flight now that large cross flow, pressure gradient, and geometry effects are present?

- Interference -- What interpretation do we place on ideal gas wind-tunnel results regarding the thermal protection design of vehicles which will fly in a real gas atmosphere?

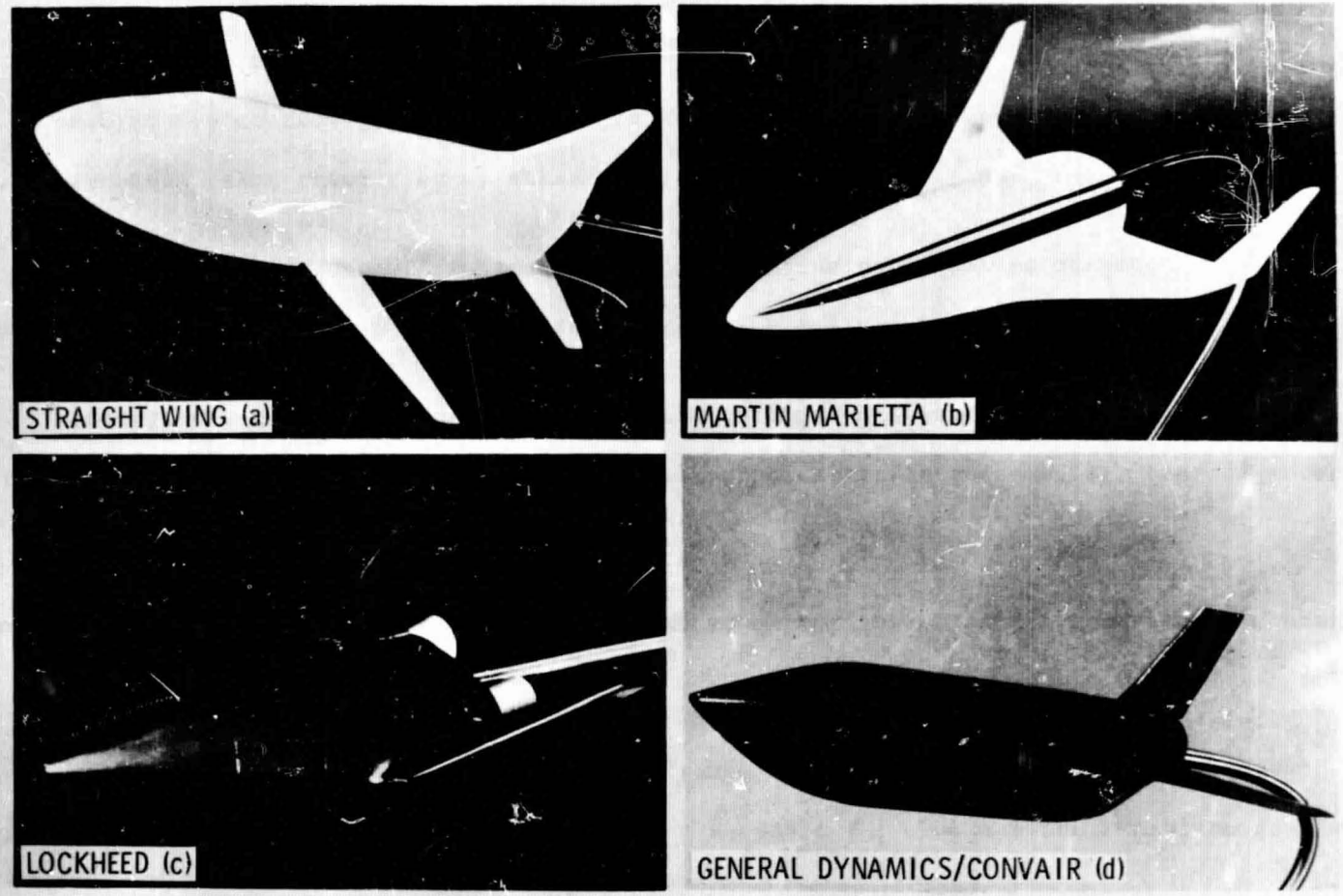

Figure 1.- Models of orbiter configurations.

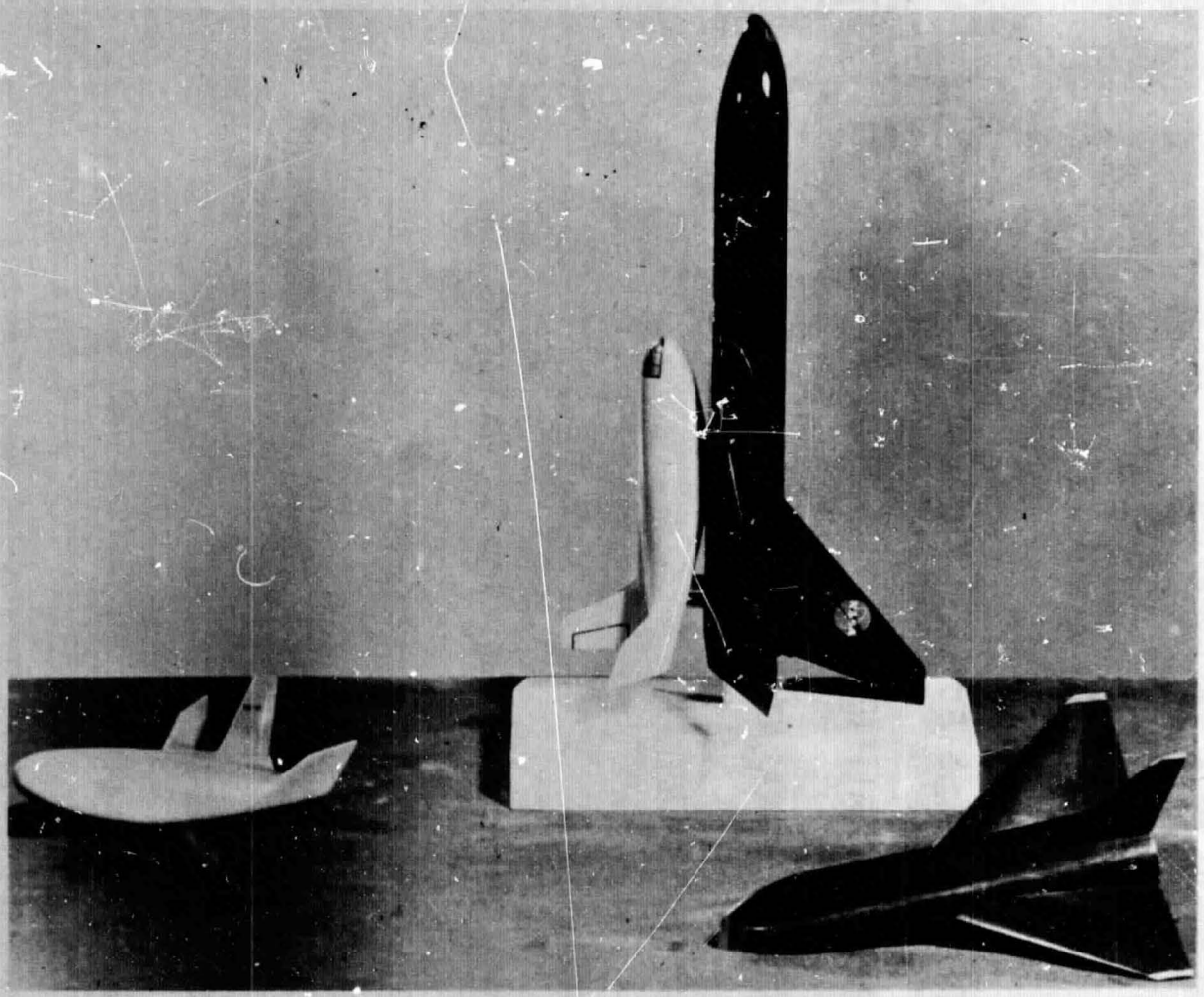

Figure 2.- Models of HL-10 orbiter and McDonnell Douglas booster.

SPACE SHUTTLE AEROTHERMODYNAMICS

PERFORMANCE, STABILITY, CONTROL

HANDLING QUALITIES

VISCOUS DEGRADATION

HEAT TRANSFER

LOADING

INTERFERENCE (LOADING, FORCES, MOMENTS, HEATING)

STAGING AND ABORT SEPARATION

B. L. CHARACTERISTICS, TRANSITION, SEPARATION

VORTEX FLOWS

TURBULENT HEATING

Figure 3.- Illustrative areas of study.

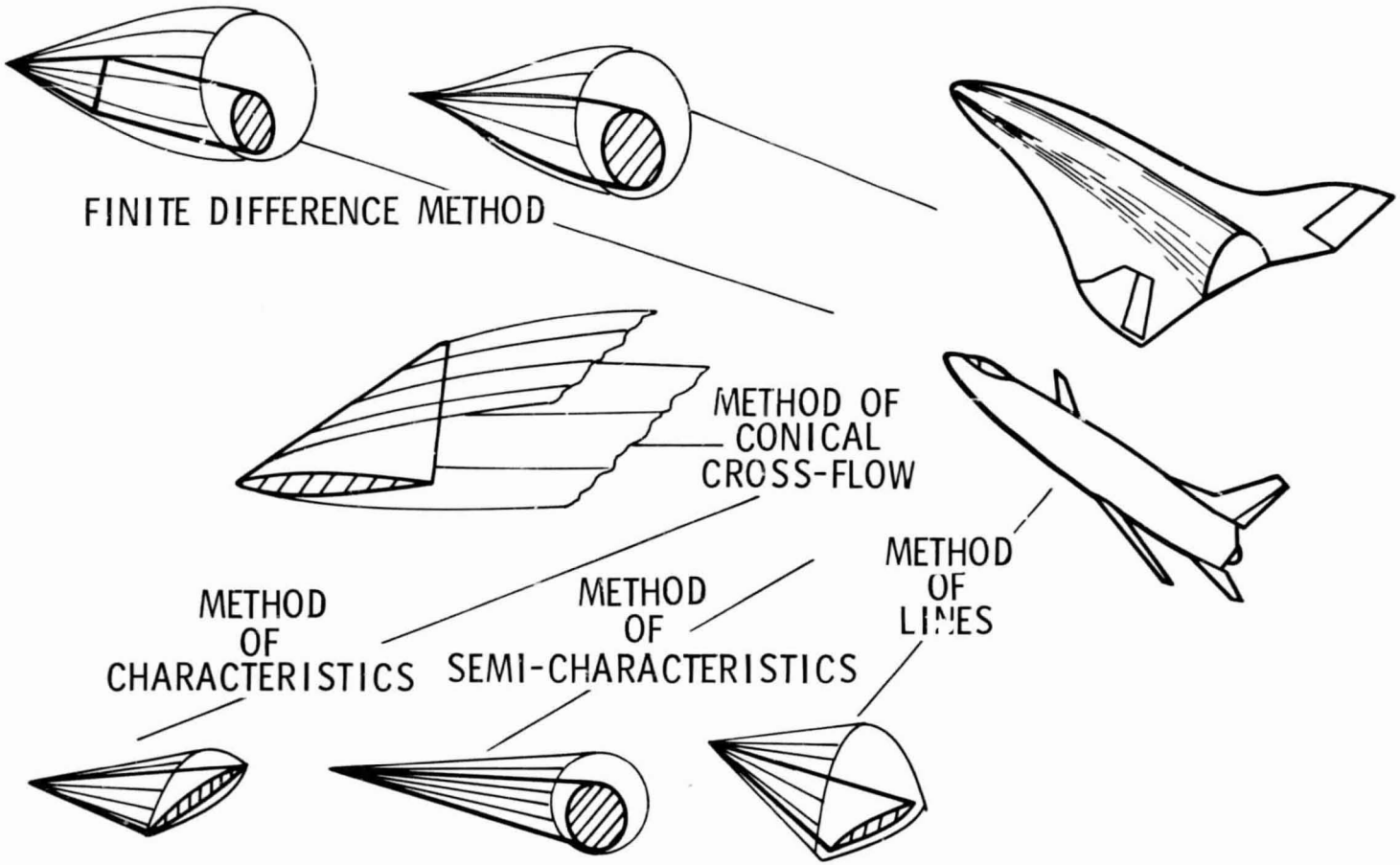

Figure 4.- Desired focus of theoretical work.

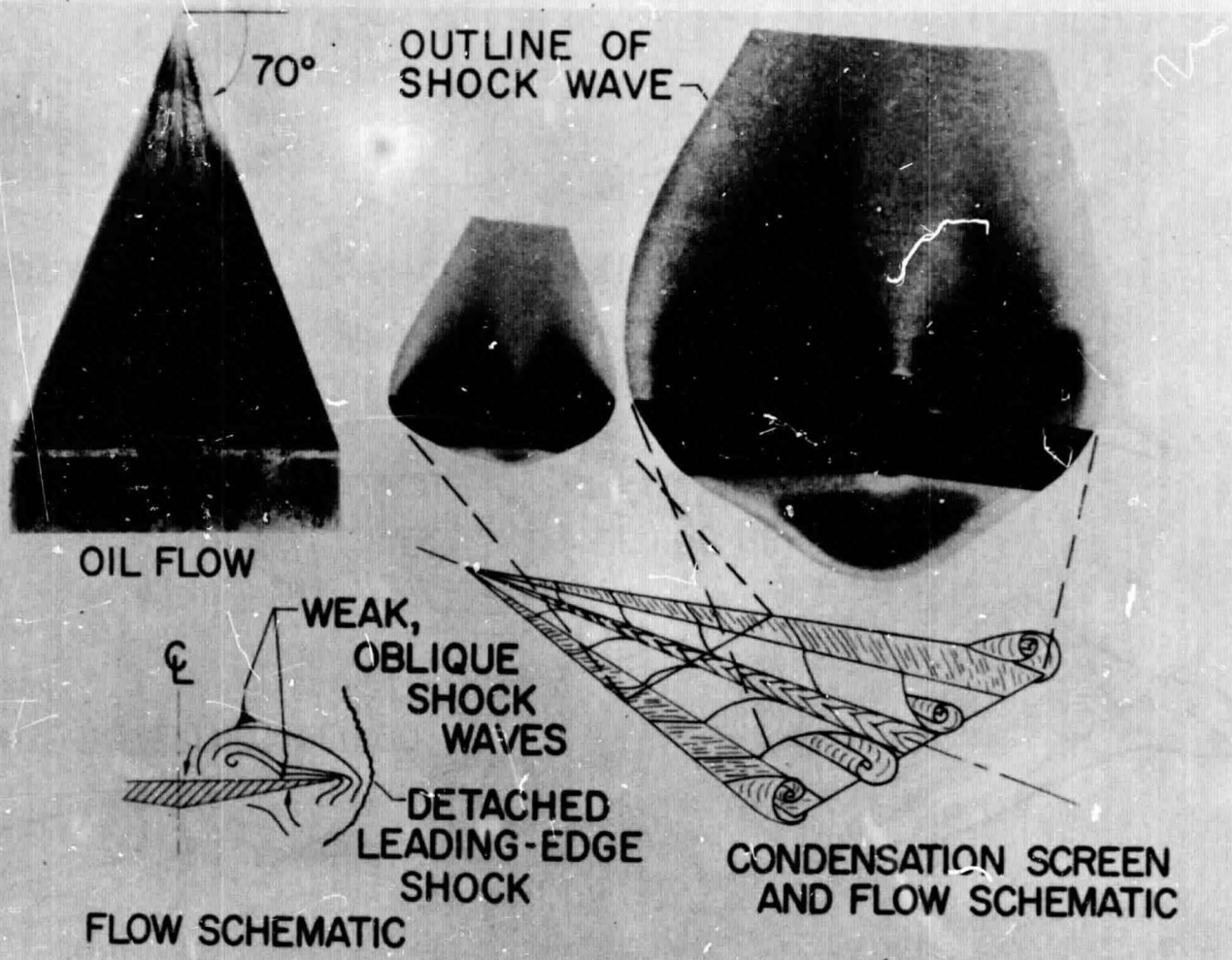

Figure 5.- Flow conditions on lee side of 70° sweep delta wing and flap; M = 6, α = -10°, δ = 0°.

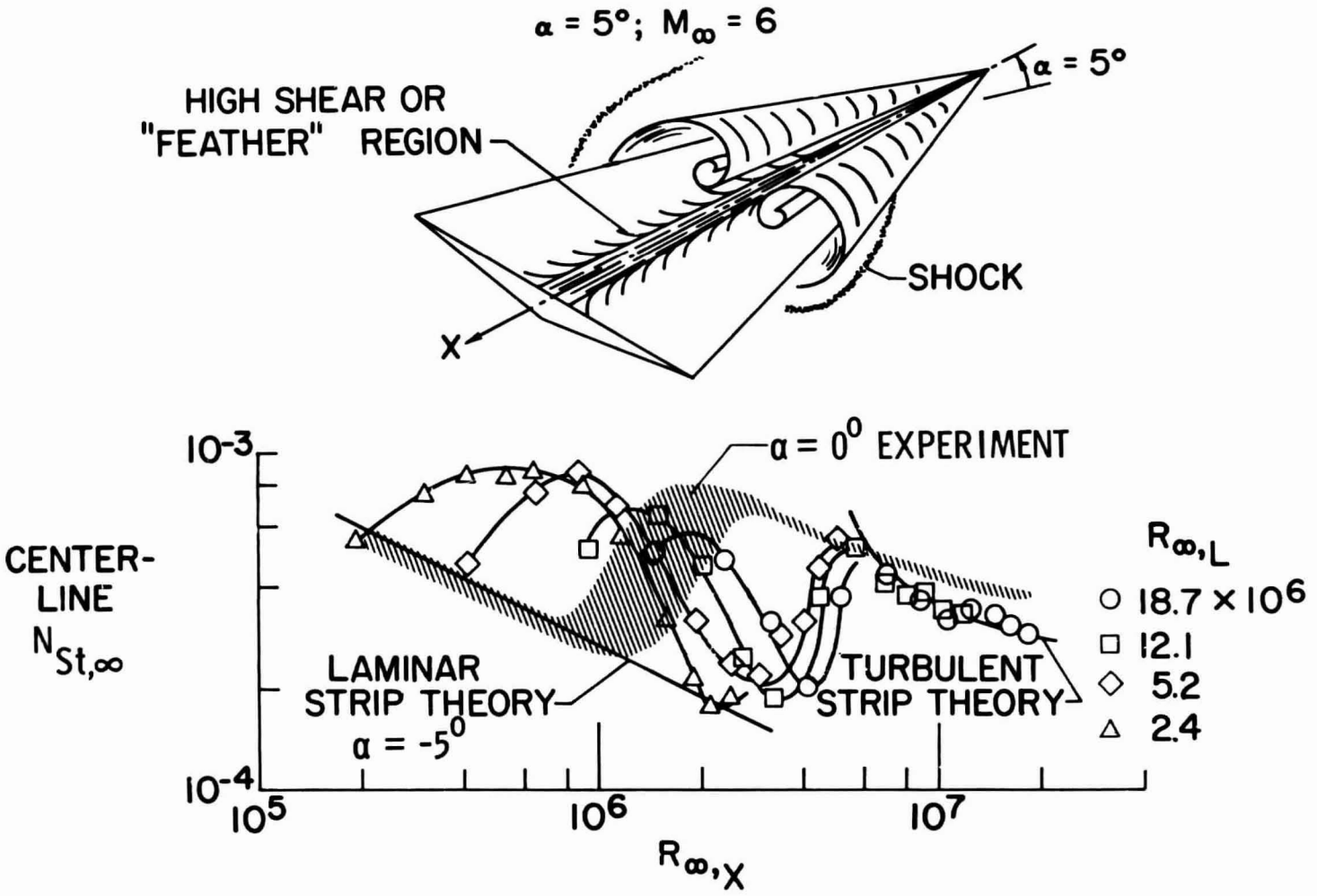

Figure 6.- Center-line heating on lee surface of delta wing; M = 6, $\alpha = 5^{\circ}$.

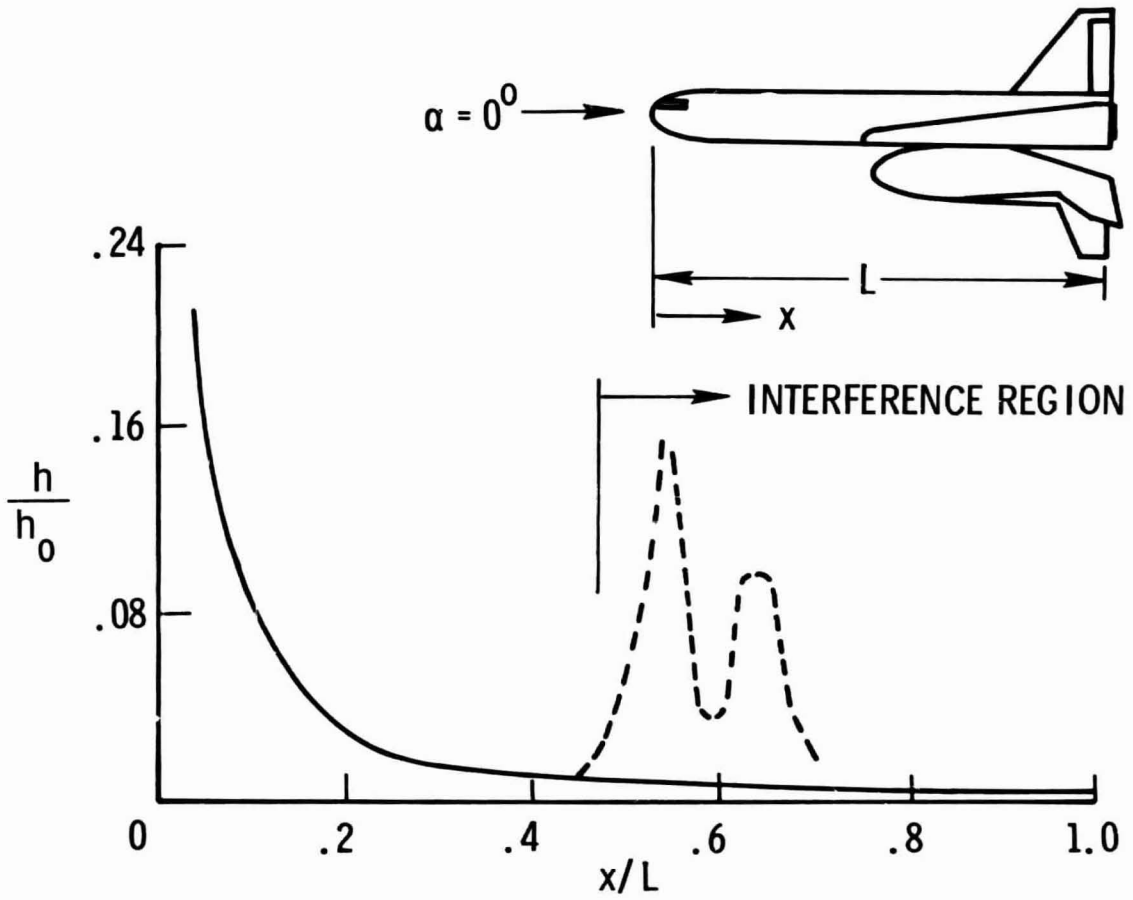

Figure 7.- McDonnell Douglas HL-10 launch configuration interference heating on McDonnell Douglas booster; M = 10.

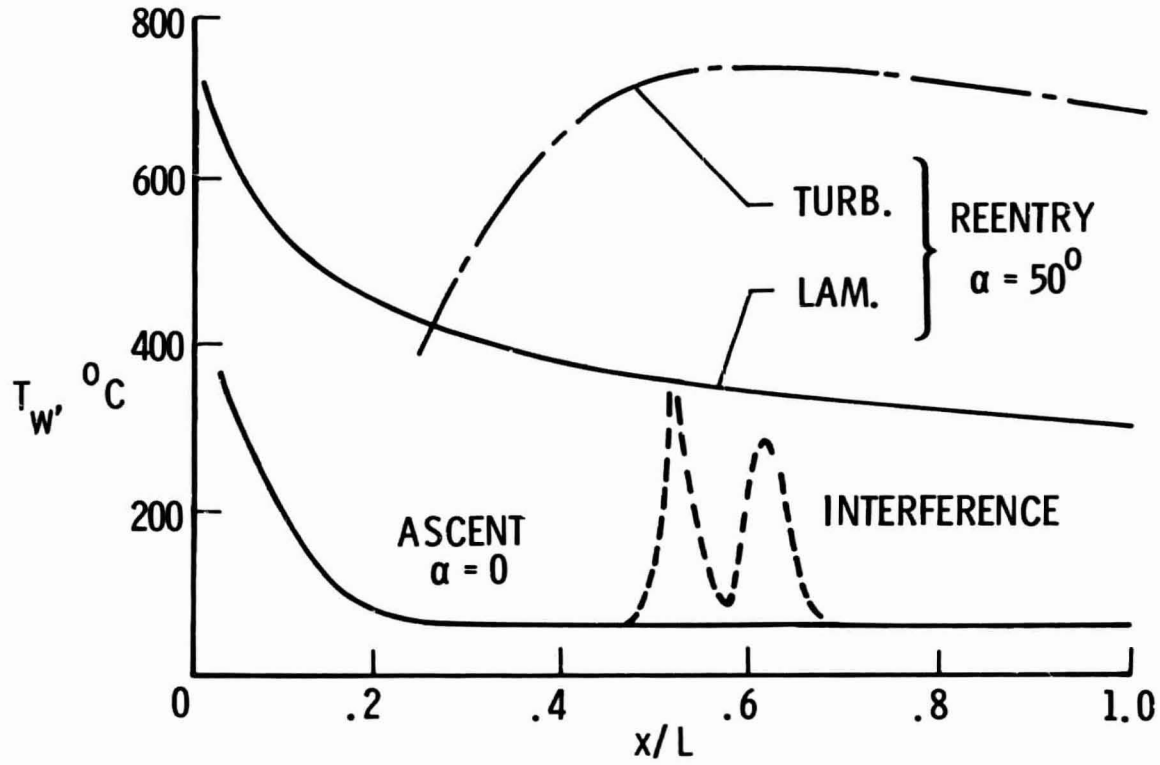

Figure 8.- McDonnell Douglas booster launch and entry phases; maximum skin temperatures.

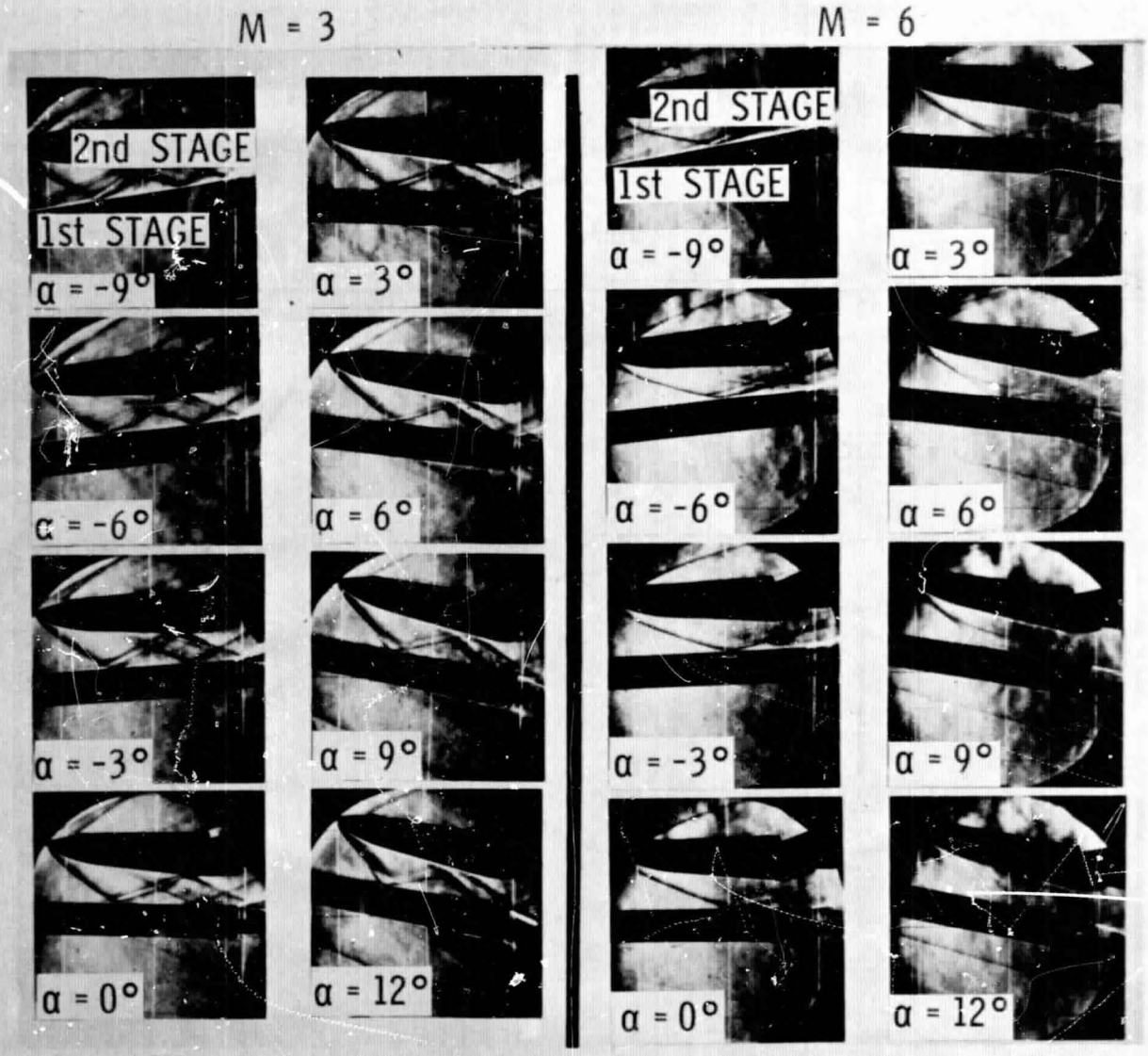

Figure 9.- Booster-orbiter separation.

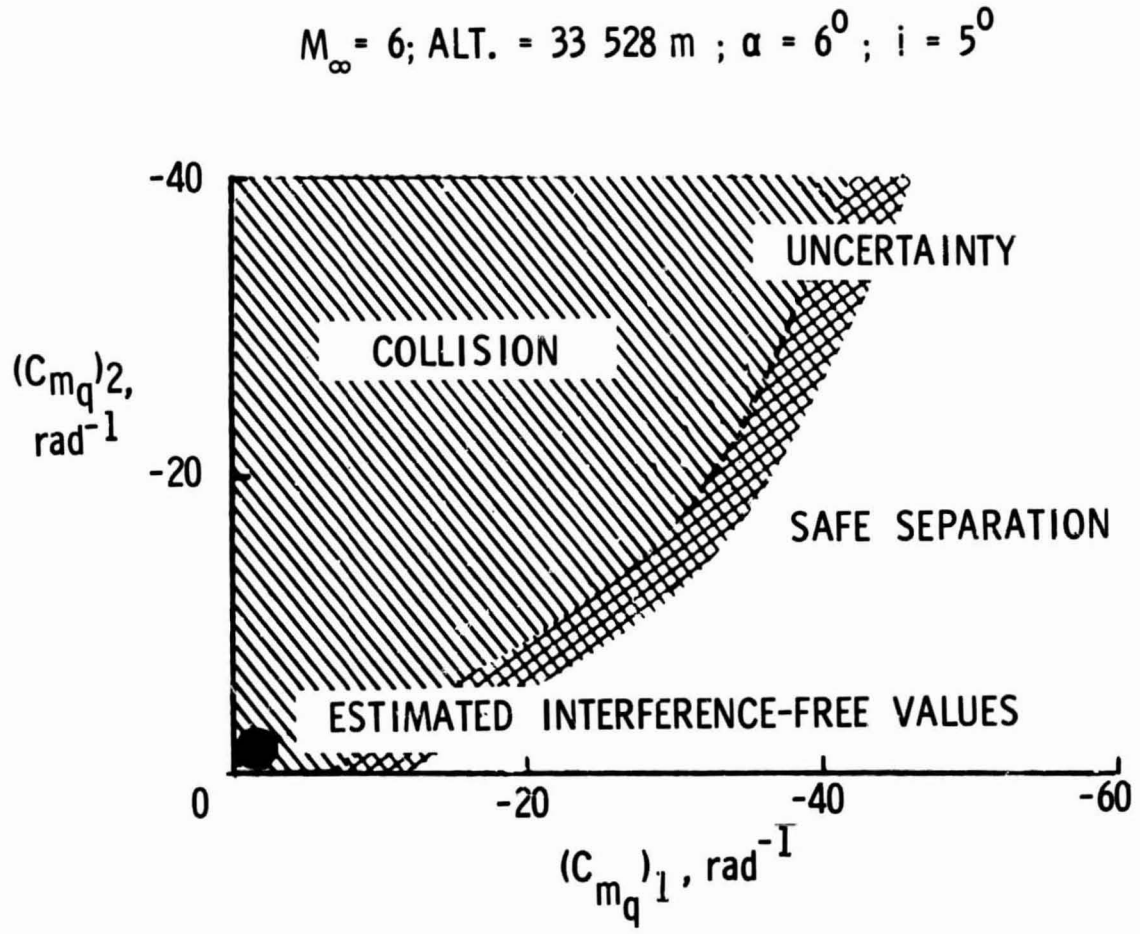

Figure 10.- Effect of dynamic derivatives on booster-orbiter separation.

STATIC AERODYNAMIC DATA : C_N ; C_m ; C_A

DYNAMIC DERIVATIVES : C_{m_q} ; $C_{m_{\dot{\alpha}}}$; C_{N_q} ; $C_{N_{\dot{\alpha}}}$

VEHICLE CHARACTERISTICS: m ; I_{yy}

LAUNCH VEHICLE TRAJECTORY QUANTITIES AT SEPARATION : h ; q ; γ ; V_c

INITIAL ATTITUDE AND POSITION OF SECOND STAGE : Δx ; Δz ; i

Figure 11.- Inputs for booster-orbiter separation trajectory program.

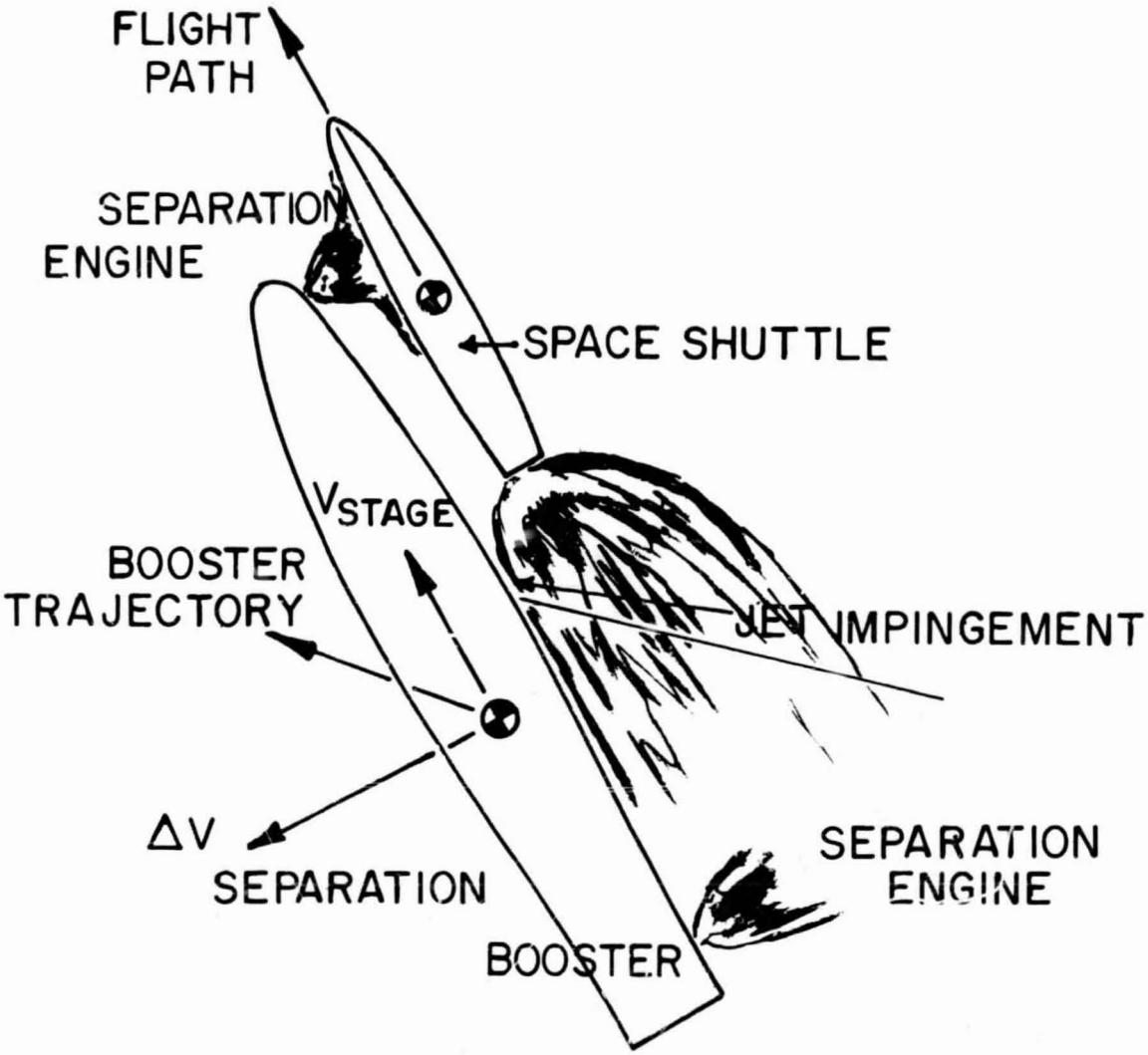

Figure 12.- Booster-orbiter separation, jet plume effect.

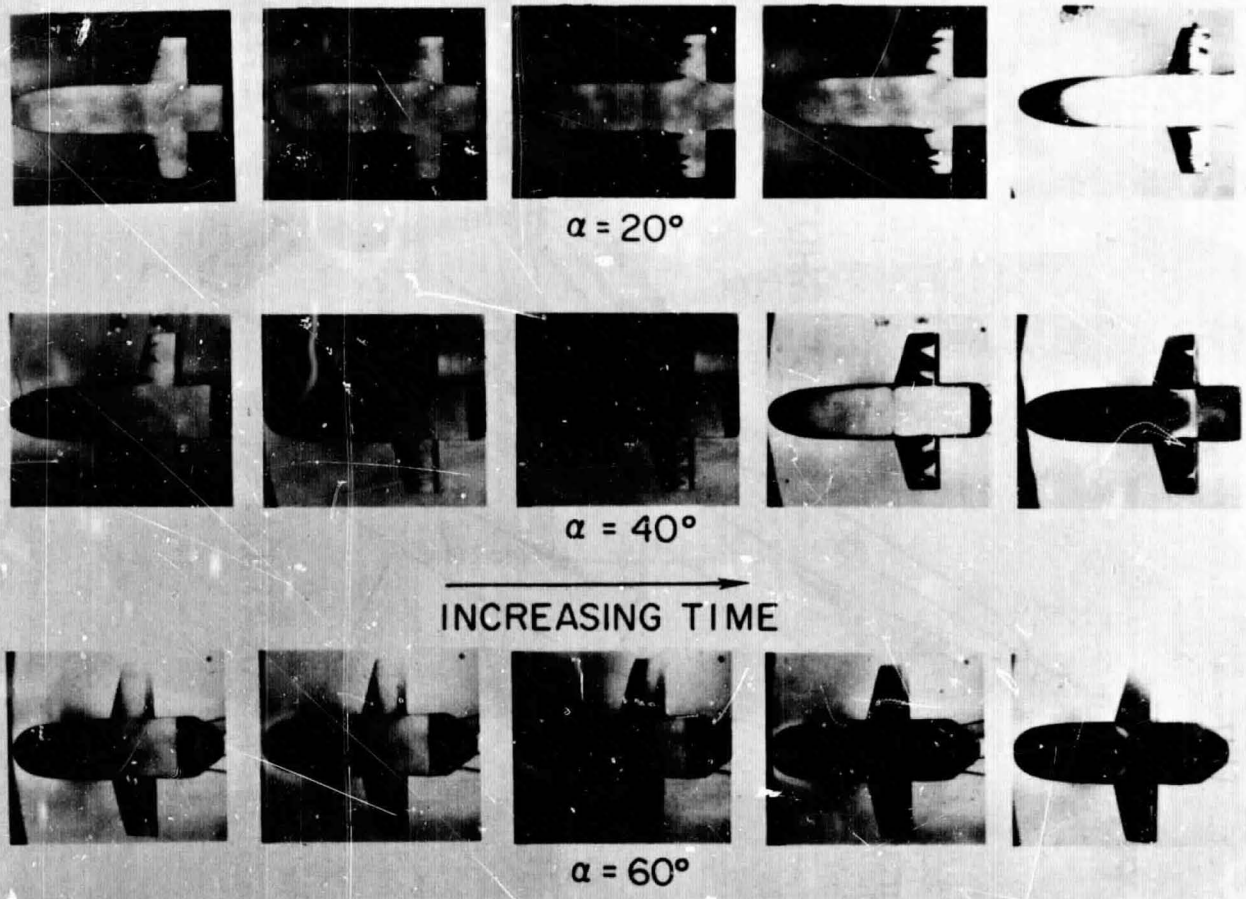

Figure 13.- Phase-change patterns on straight wing orbiter; M = 10.

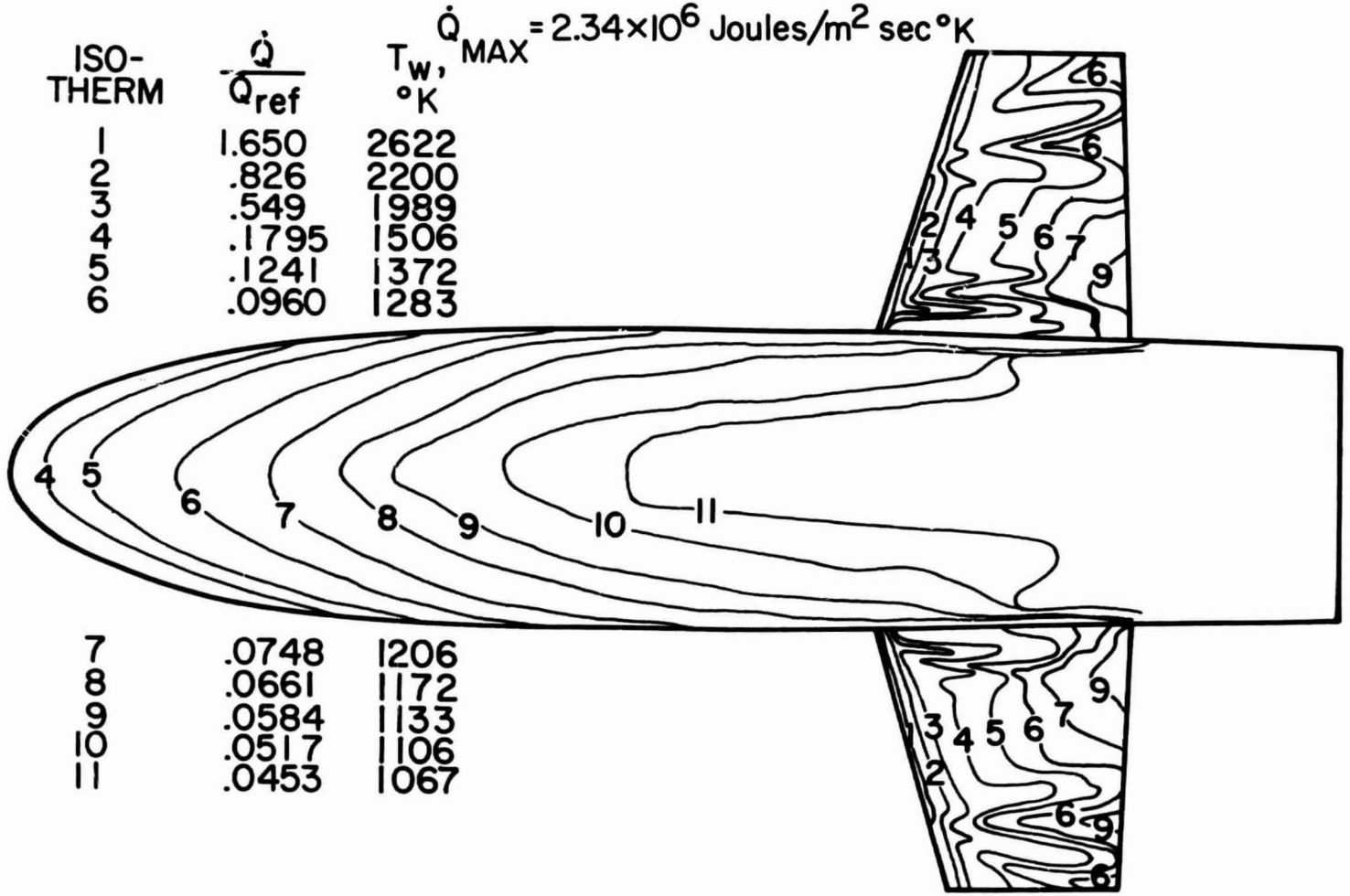

Figure 14.- Straight wing orbiter maximum heat transfer and equilibrium skin temperature, constant $\alpha = 20^{o}$ entry trajectory; M = 8.

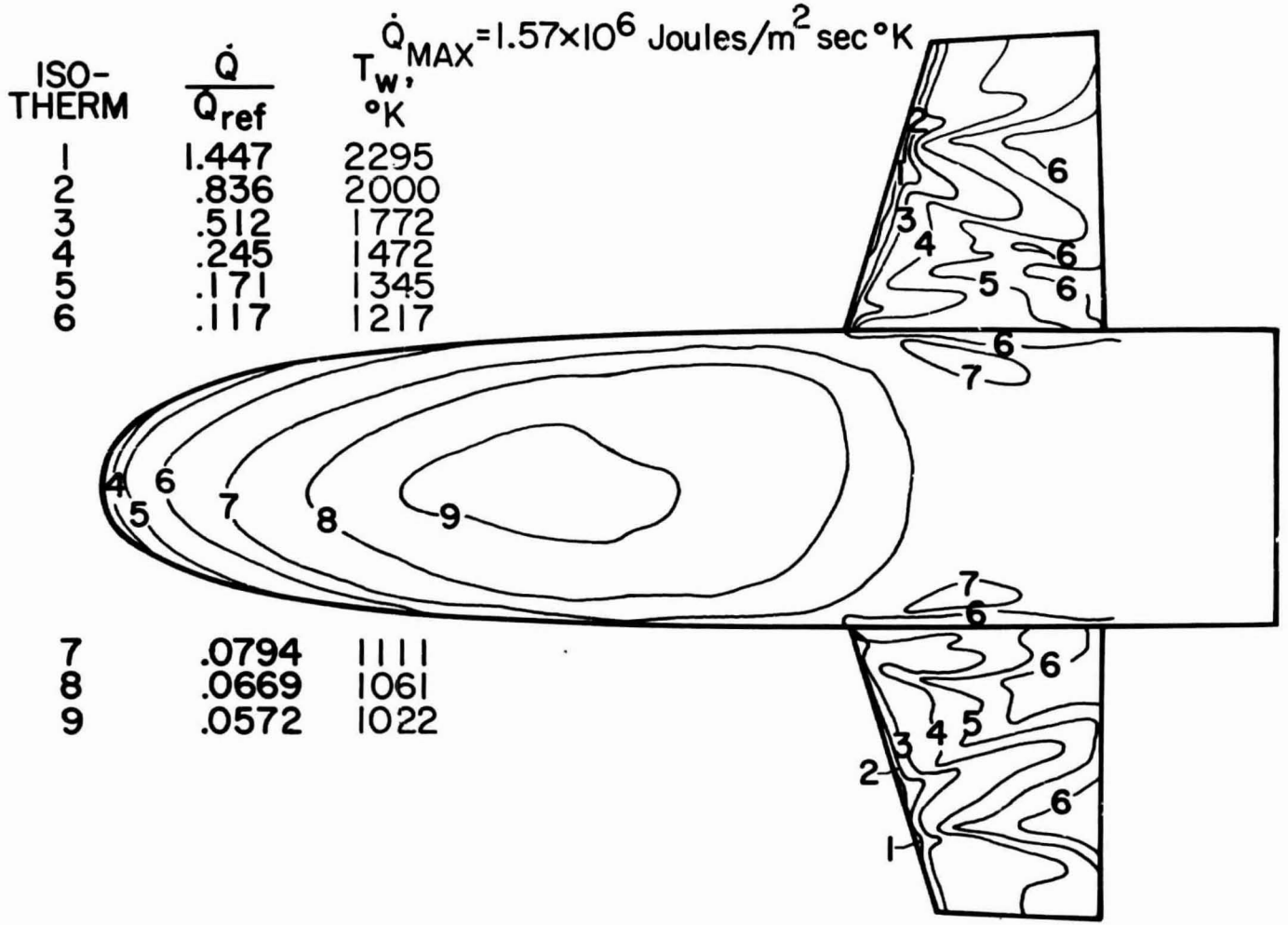

Figure 15.- Straight wing orbiter maximum heat transfer and equilibrium skin temperature, constant $\alpha = 40^{o}$ entry trajectory; M = 8.

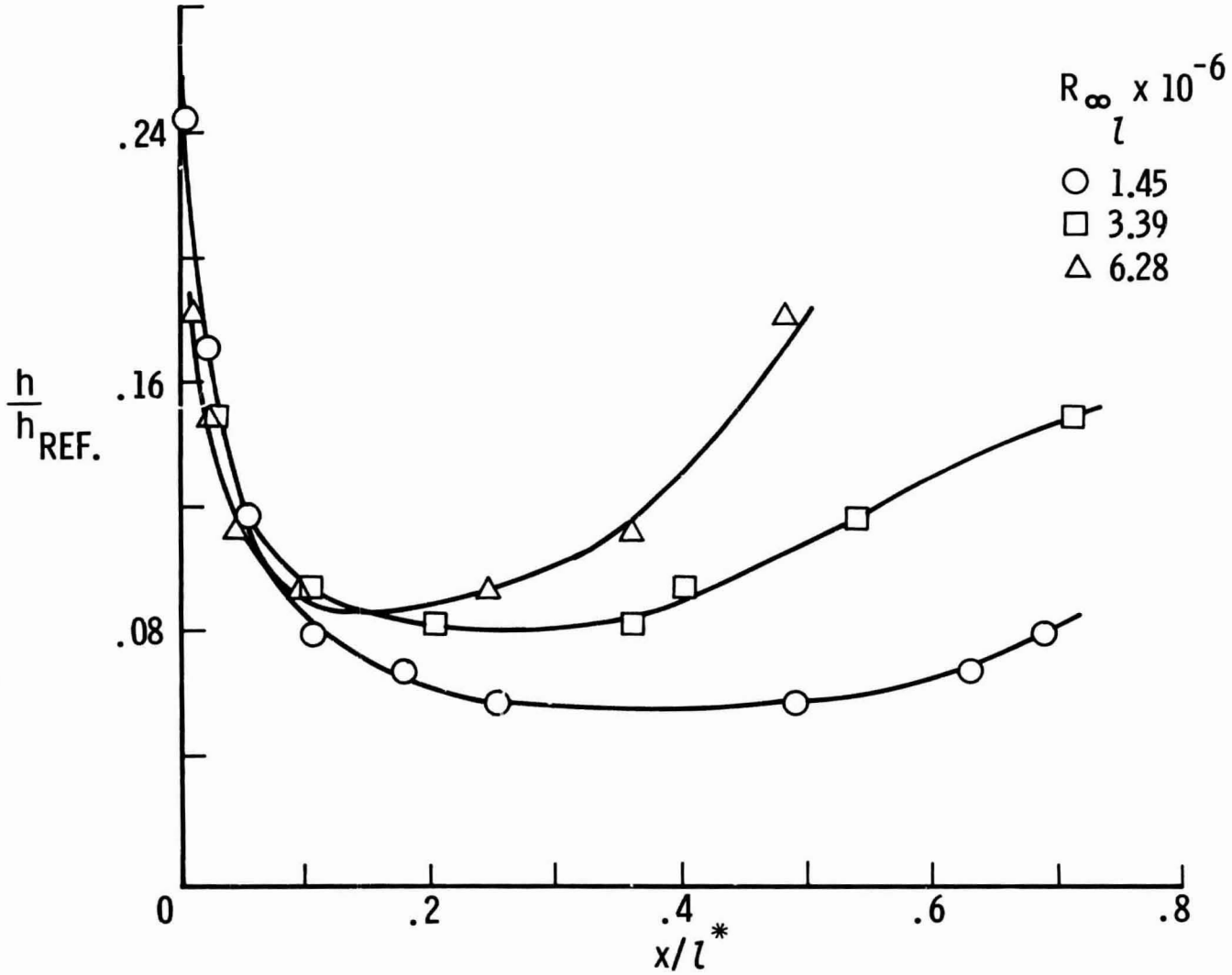

Figure 16.- Windward center-line heat-transfer distribution, straight wing orbiter; $\alpha = 40^{\circ}$.

α	$R_{\infty} \times 10^{-6}$ / ℓ	M_e	$\frac{\rho_e u_e s}{\mu_e}$
20°	1.45	-	-
20°	3.39	-	-
20°	6.28	2.10	$.410 \times 10^6$
40°	1.45	1.10	$.075 \times 10^6$
40°	3.39	1.04	$.110 \times 10^6$
40°	6.28	.91	$.150 \times 10^6$

Figure 17.- Windward boundary-layer transition conditions, center line of straight wing orbiter.

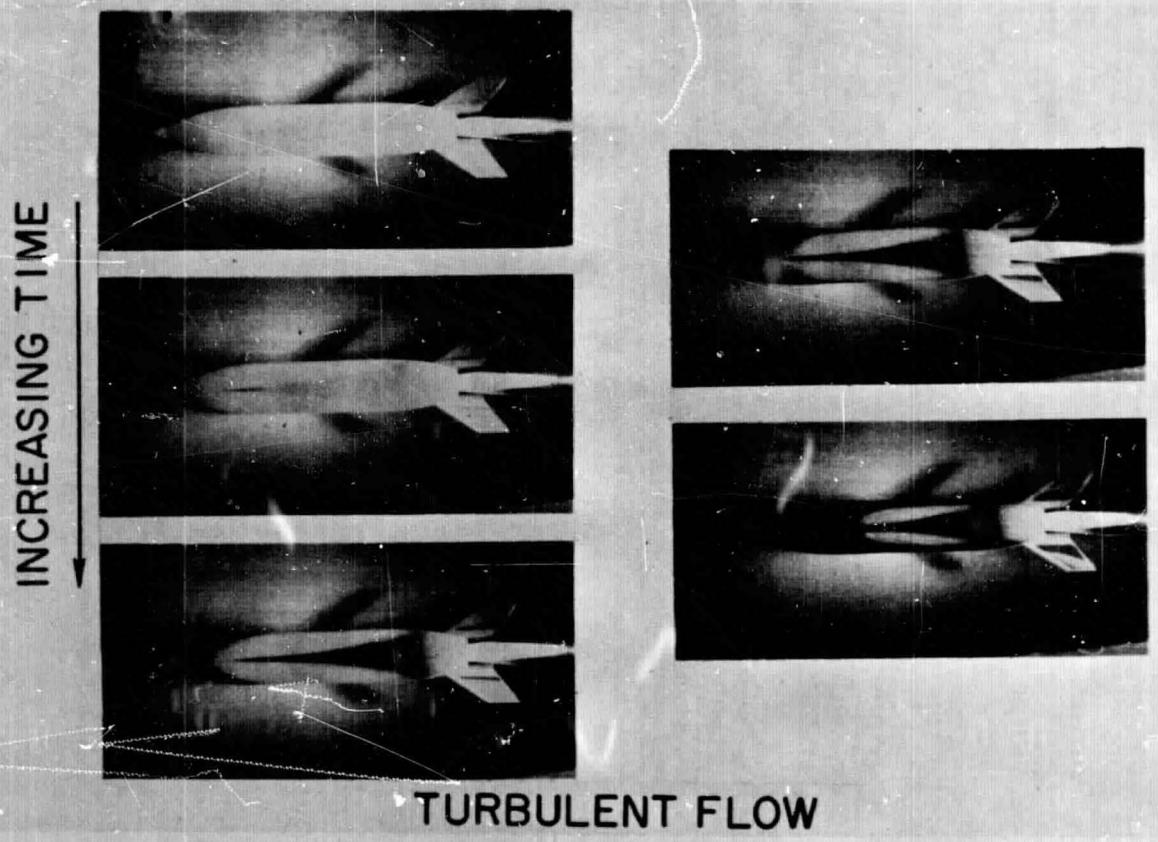

Figure 18.- General Dynamics/Convair orbiter phase-change patterns, bottom view; M = 8, α = 25°.

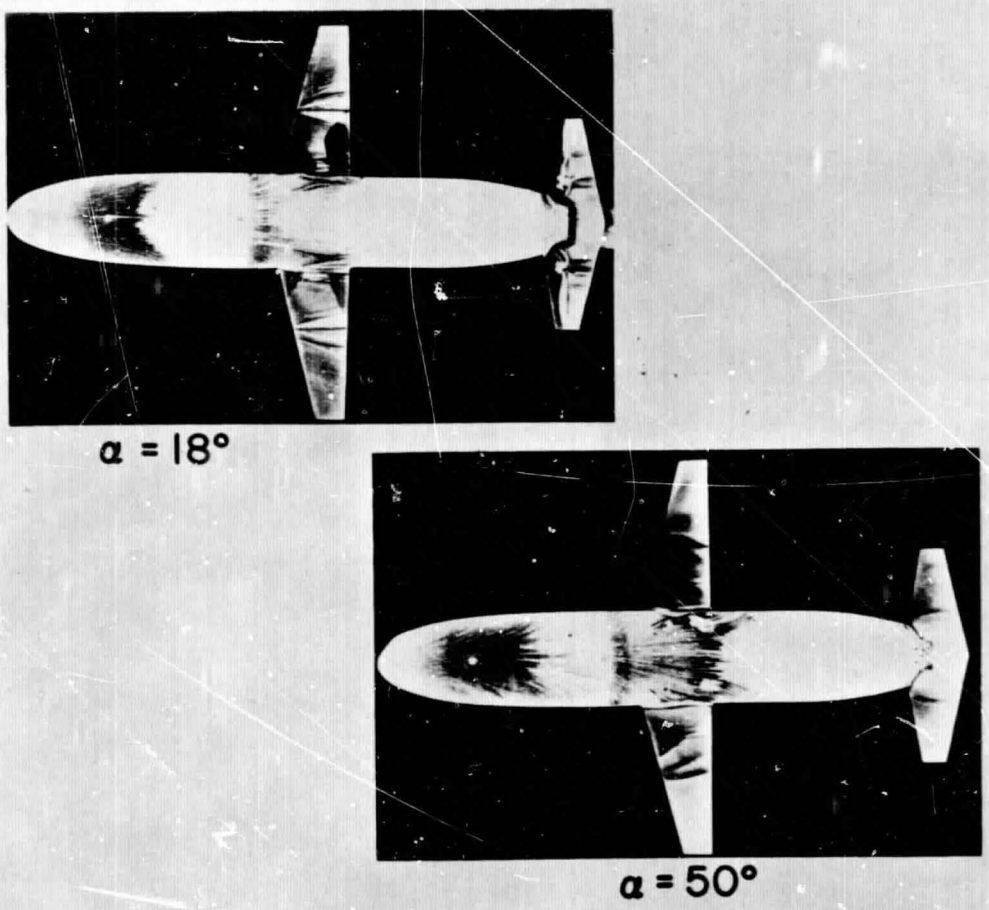

Figure 19.- Straight wing orbiter lower surface oil flow patterns; M = 7.4.

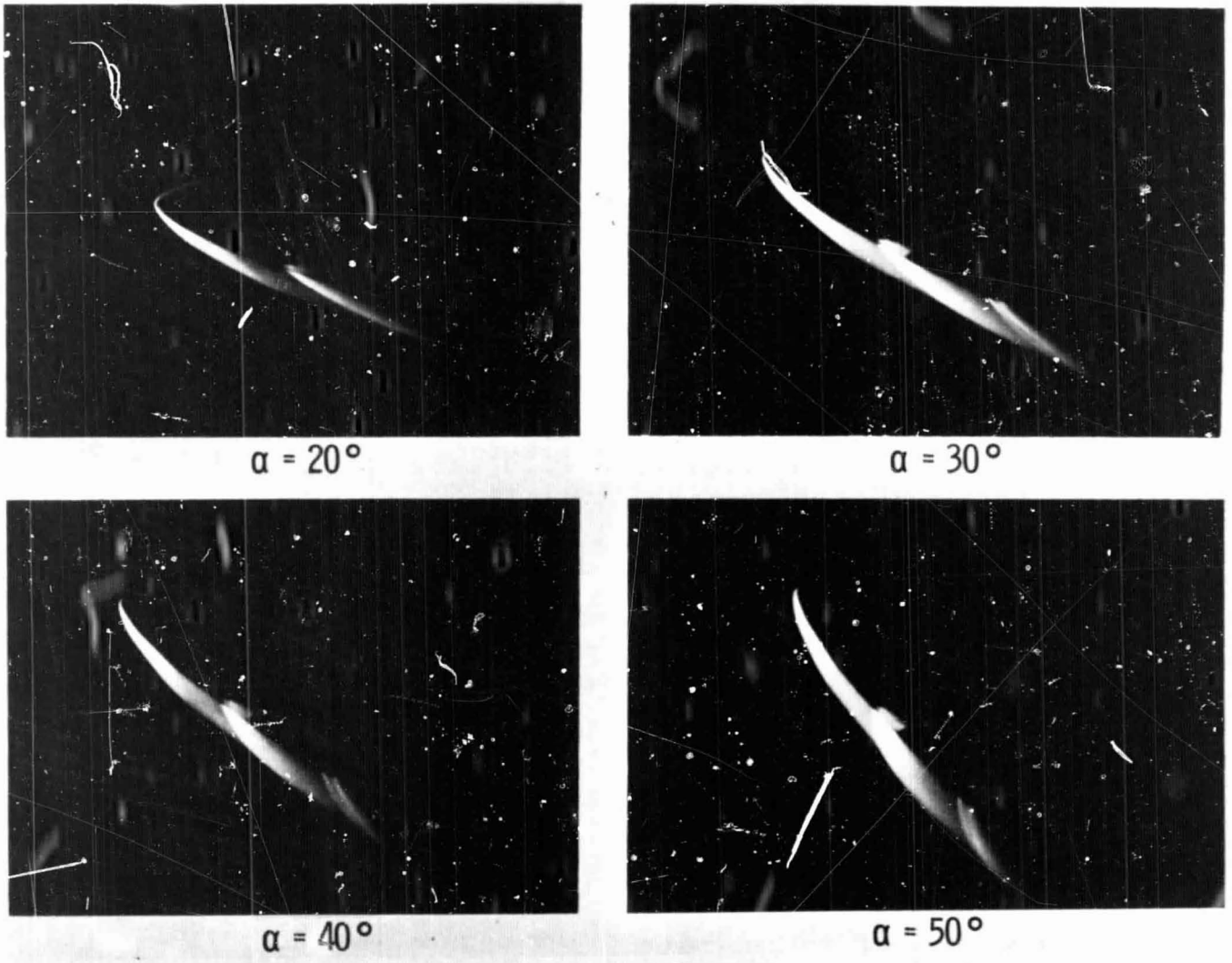

Figure 20.- Straight wing orbiter internal shock structure; M = 20.

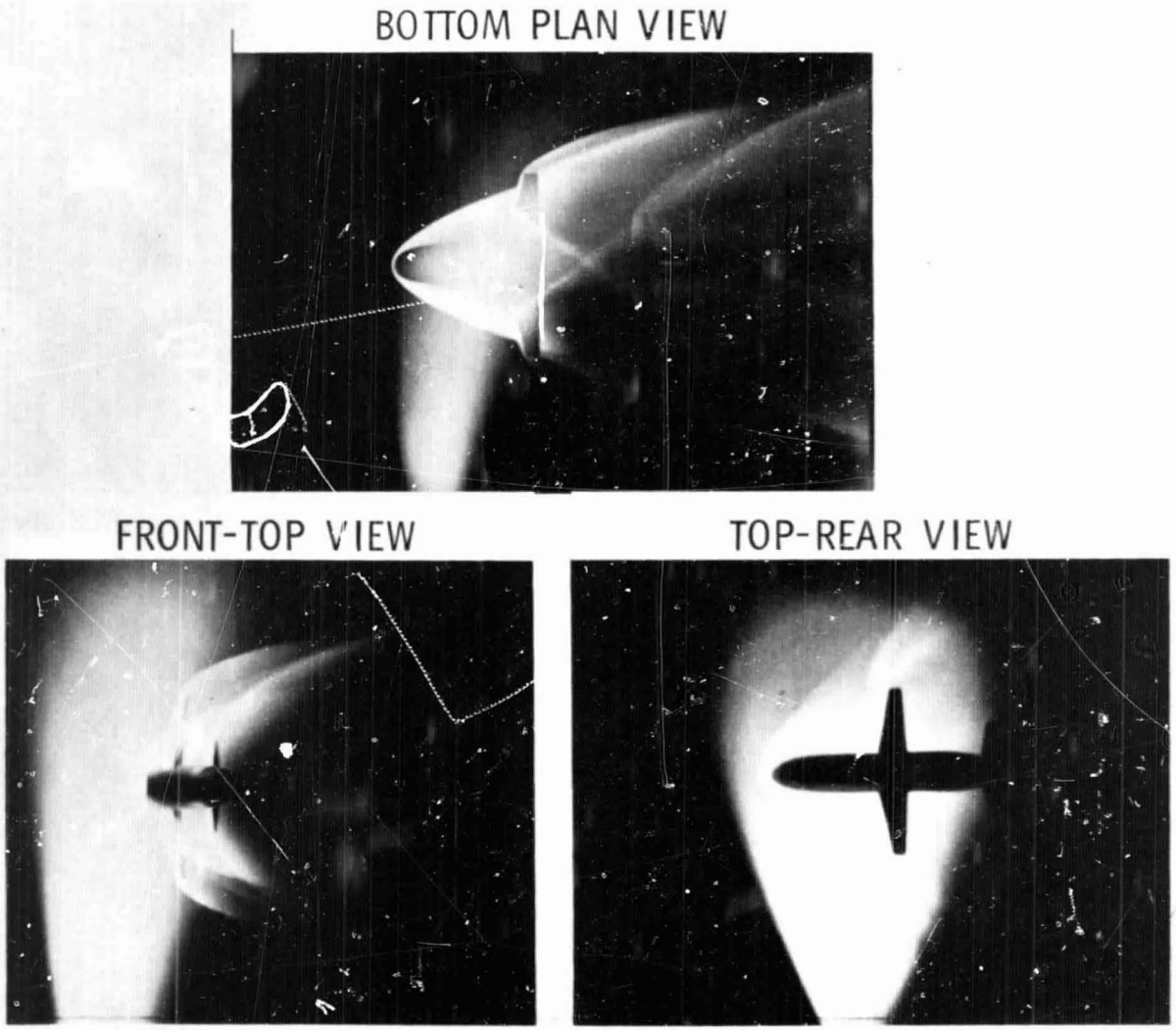

Figure 21.- Straight wing orbiter shock interference pattern; M = 20, $\alpha = 40^{\circ}$.